JMST

by Hendriko 1

Submission date: 18-Jun-2021 08:00AM (UTC+0700)
Submission ID: 1608286466
File name: finish_five-axis_milling_of_nonstraight_staircase_workpieces.pdf (2.38M)
Word count: 6407
Character count: 32365

KSME

Springer

Journal of Mechanical Science and Technology 34 (3) 2020

Original Article
DOI 10.1007/s12206-020-0229-x

Keywords:
· Analytical method
· Cut geometry
· Five-axis milling
· Semi-finish milling

Correspondence to:
Hendriko Hendriko
hendriko@pcr.ac.id

Citation:
Hendriko, H. (2020). Cut geometry calculation for the semifinish five-axis milling of nonstraight staircase workpieces. Journal of Mechanical Science and Technology 34 (3) (2020) ?~?.
http://doi.org/10.1007/s12206-020-0229-x

Received June 11th, 2019
Revised January 5th, 2020
Accepted January 12th, 2020

† Recommended by Editor Hyung Wook Park

Cut geometry calculation for the semifinish five-axis milling of nonstraight staircase workpieces

Hendriko Hendriko

Mechatronic Department, Politeknik Caltex Riau, Pekanbaru 28265, Indonesia

Abstract The cut geometry prediction, especially the issue regarding computational time, of a complex part surface in five-axis milling remains as a challenge. In this study, the analytical boundary method, which was developed to predict the cut geometry during semifinish milling, was extended by adding a curve boundary algorithm. The extended algorithm made the method applicable not only for workpieces with a straight staircase profile but also for those with a nonstraight one. The proposed method was tested using two parts with different surface shapes. Results demonstrated that the proposed method is applicable for defining instantaneous cut geometry. The verification test proved that the method was accurate when the engagement point was on the top and straight wall surfaces. Relatively small errors were observed when the engagement point was on the nonstraight surface. Moreover, the test on computational time verified the efficiency of the developed method.

1. Introduction

Many researchers are developing virtual machining applications that can be used to predict machining processes and performance. One of the main performance indicators that is widely studied in milling processes is the cutting force. An accurate and efficient method for cutting force prediction is required to optimize the machining process. Lee and Cho [1] classified the method to calculate cutting forces into three categories: Analytical, numerical, and mechanistic. However, Gao et al. [2] stated that the analytical approach is less accurate, and the numerical one is time consuming; they preferred the mechanistic approach because of its intermediate advantages under different cutting conditions and cutter types. When using a mechanistic approach, three variables are essential in calculating cutting forces. These variables are cutting force coefficients, instantaneous cut thickness, and in-cut segment of the cutting edge, which is also called the length of cut. The cutting force coefficients are obtained through experimental calibrations for a specific workpiece material-tool geometry pair. Numerous studies have been performed to define these coefficients.

Given that the cutting force coefficients are constant for a specific workpiece material and tool geometry, the cutting forces are strongly influenced by chip thickness and length of cut. Merdol and Altintas [3] stated that identifying the cut geometry is one of the crucial challenges in predicting cutting forces. Many studies have been performed to develop an accurate method to calculate chip thickness. Wojciechowski et al. [4] developed a cutting force model based on the finite element method and mechanistic approach during microend milling. The uncut chip thickness was calculated by considering the effects of runout and tool deflection. Zhang et al. [5] proposed a method for predicting the uncut chip thickness of a complex tool path during five-axis flank milling by considering the effect of cutter runout. Nikawa et al. [6] evaluated the machining method for controlling chip thickness through a simulation based on NC data. The objective of this technique is to modify the NC data and improve the machinability. The test on a complex surface milling showed that the method significantly reduced the machining time.

In this study, the cut geometry calculation was focused on developing the method to calculate

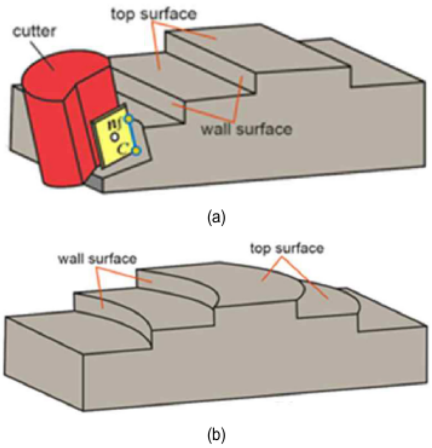

Fig. 1. Typical illustration of a workpiece surface from rough milling: (a) Straight; (b) nonstraight staircase.

the length of cut. According to Zheng et al. [7], the length of cut exerts the greatest effect to the cutting forces, whereas feed rate, which influences the chip thickness, exerts the greatest effect to surface roughness.

In five-axis milling, two prominent methods can be used to define the cutter workpiece engagement (CWE): Solid model and discrete method. Numerous studies on the establishment of the solid model for CWE extraction have been reported. Yip-Hoi and Huang [8] developed a solid modeler-based approach for calculating the cutter engagement features for the case of a 2.5D milling process. Lazoglu et al. [9, 10] used a boundary representation-based method to determine the chip load. Boolean operations were used to subtract the tool-workpiece intersection. The solid model is widely used because this model accurately defines the CWE extraction of complex parts using Boolean operations. However, the solid model is limited in terms of computational time, especially during free-form machining.

Therefore, several researchers used discrete methods, such as Z-mapping, Z-buffer, and polyhedral model, to define the intersection area between the workpiece material and the cutting tool. Yun et al. [11] developed the moving edge-node Z-map model to calculate the continuous variable of the cutting configurations with a given NC code. Zhang et al. [12, 13] developed another type of Z-mapping method called the depth element approach. Fussel et al. [14] developed an extended Z-buffer model to represent the workpiece. The CWE was determined by the intersection between the swept envelope of the tool path and the Z-buffer element of the workpiece. The advantage of the Z-mapping and Z-buffer methods is efficiency in the rendering process; however, the control on geometric accuracy is low.

Another discrete method for modeling CWE is the polyhedral model. In this model, the workpiece surfaces are represented by a finite set of polygonal planes called facets [15, 16]. The polyhedral modeling offers a good compromise between manageable computational speed, robustness, and accuracy.

In general, the discrete method cannot obtain an accurate result in comparison with the solid model because of the rasterization problem, which is present in many applications of the discrete method [11]. Nevertheless, the issue on accuracy can be solved by sharpening the resolution. However, this solution leads to long computational time.

To solve the problem of long computational time, several researchers proposed analytical methods. Gupta et al. [17] proposed an analytical method for determining the CWE of 2.5D machining. They mentioned that the analytical method is cheaper and more precise compared with the discrete method. Ozturk and Lazoglu [18] developed an analytical method to define the cut geometry of three-axis milling using a ball end mill. Tunc and Budak [19] proposed a simple analytical method for five-axis milling called bounding point coordinate. Although this method is accurate and simple, the validity only applies to flat workpiece surfaces. Zhang et al. [20] developed the method to predict the cutting force in the five-axis flank milling of a sculptured surface. The proposed method considered the curved tool path and the actual tool motion with cutter runout. However, this method could only define the length of cut of flat workpiece surfaces.

Kiswanto et al. [21, 22] developed a hybrid analytical and discrete method for calculating the cut geometry during sculptured surface machining using a flat-end mill. This method is suitable for finish milling but not when the workpiece has a staircase surface profile (Fig. 1).

Previous studies have proposed an analytical method for obtaining the cut geometry during semifinish milling [23-25]. The proposed method is called the analytical boundary method (ABM). The implementation of ABM was established and tested to support the calculation of the cutting forces [26]. The method was further developed to define the scallop height of a complex machining process [27]. The verification tests proved that the method is accurate and computationally fast. The cut geometry was determined by identifying two engagement points, namely, lowermost and uppermost engagement points (LEP and UEP, respectively). The developed method was proven accurate and cheap in terms of computation. However, this algorithm was only applicable for workpieces with straight staircase profiles (Fig. 1(a)). For a complex part, rough milling could be performed using different strategies so that the thickness of the material during finish milling remains relatively consistent. Hence, the shape of the workpiece surface can follow a nonstraight staircase profile (Fig. 1(b)) instead of a straight one depending on the machining strategy selected during rough milling.

Therefore, the method for defining the cut geometry for semifinish five-axis milling was extended in this study. The algorithm was developed to apply ABM to nonstraight staircases. The profile of the wall surface in every stair level in one tool pass was expressed using the coordinate of the six points located on the top of the wall surface. Then, the shape of the stair surface

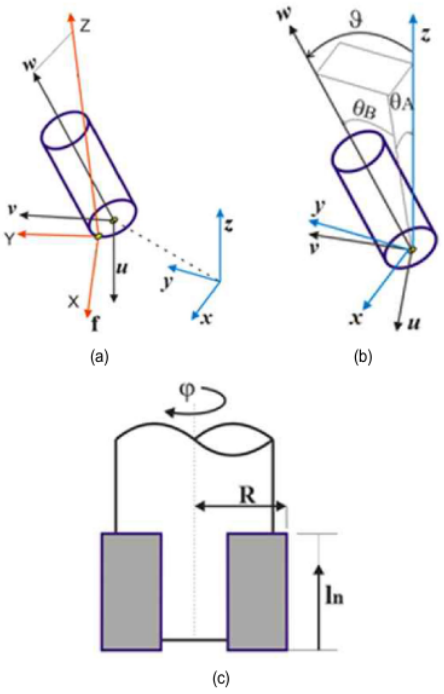

Fig. 2. (a) Geometry of a flat-end cutting tool; (b) tool orientation relative to GCF; (c) geometry of a flat-end cutting tool [23].

was defined using a polynomial equation based on the coordinate of the points on the top of the wall surface. The details of the mechanism are discussed in the following sections.

2. Tool geometry and orientation

The two additional degrees of freedom (DOFs) is the advantage of five-axis milling over the three-axis one. These additional DOFs allow the cutting tool to be rotated to an arbitrary direction. Machining a complex part can be efficiently performed by controlling the dynamic tool movement with respect to the part surface normal. However, the additional DOFs also increase the difficulty of programming and simulating the machining process.

For analysis, coordinate systems and corresponding transformation mechanisms should be established. The coordinate systems have been established in a previous study [23]. Three coordinate systems were used to define the posture of the cutter (Fig. 2(a)): Global coordinate frame (GCF), tool coordinate frame (TCF), and local coordinate frame (LCF). GCF was defined using the base vector *x, y, z*, whereas TCF and LCF were expressed using *u, v, w* and *X, Y, Z*, respectively. The orientation of the cutting tool with respect to GCF ( ) is illustrated in Fig. 2(b). This orientation was determined using the tool orientation relative to the *x*- (θ_A) and *y-axes* (θ_B).

$$\vartheta = \cos^{-1}\left(\cos\theta_A \cos\theta_B\right) \tag{1}$$

In this study, GCF was used as a reference coordinate system. Then, the coordinate of the cutting tool in TCF was mapped to the GCF. The mapping process was performed using the mapping operator [M], which includes the tool rotation about the x- and y-axes, as well as the tool movement at $T\left(x_T, y_T, z_T\right)$.

$$[M] = \begin{bmatrix} \cos\theta_B & 0 & \sin\theta_B & x_T \\ \sin\theta_A \sin\theta_B & \cos\theta_A & -\sin\theta_A \cos\theta_B & y_T \\ \cos\theta_A \sin\theta_B & \sin\theta_A & \cos\theta_A \cos\theta_B & z_T \\ 0 & 0 & 0 & 1 \end{bmatrix}, \tag{2}$$

where $T\left(x_T, y_T, z_T\right)$ is placed at the bottom center of the cutting tool, which is defined as the cutter location point.

In this study, the cut geometry model was developed for machining using a flat-end cutter. The engagement point on the flat-end cutter in TCF was defined using the parametric equation of a cylinder.

$$S_C\left(\varphi; l_n\right) = \begin{bmatrix} R\sin\varphi & R\cos\varphi & l_n \end{bmatrix}^{\mathrm{T}}, \tag{3}$$

where R is the radius of the cutting tool, φ is the tool rotation angle, and l_n is the height of the engagement point measured from the bottom (Fig. 2(c)). The cutting-tool surface was converted from TCF to GCF because GCF was used as the reference coordinate frame.

$$S_C'\left(x_{S_C}', y_{S_C}', z_{S_C}'\right) = [\mathrm{M}]\, S_C\left(\varphi; l_n\right) \tag{4}$$

3. Wall surface representation

As previously mentioned, the wall surface is represented by a curve defined using polynomial interpolation. The algorithm developed in this study can be used to define straight and non-straight staircases. In this study, the shape of the curve, which represents the shape of the wall surface, was constructed using a fifth-degree polynomial based on six given points; the shape is expressed as

$$x_j = H_{0j} + H_{1j} y_j + H_{2j} y_j^2 + H_{3j} y_j^3 + H_{4j} y_j^4 + H_{5j} y_j^5, \tag{5}$$

where $j(1,\ldots,n)$ represents the order of the workpiece section. To define the value of H_{0j}, H_{1j}, ..., H_{5j}, the matrix form of the six linear equations is generated as

$$\begin{bmatrix} 1 & y_{0j} & y_{0j}^2 & y_{0j}^3 & y_{0j}^4 & y_{0j}^5 \\ 1 & y_{1j} & y_{1j}^2 & y_{1j}^3 & y_{1j}^4 & y_{1j}^5 \\ 1 & y_{2j} & y_{2j}^2 & y_{2j}^3 & y_{2j}^4 & y_{2j}^5 \\ 1 & y_{3j} & y_{3j}^2 & y_{3j}^3 & y_{3j}^4 & y_{3j}^5 \\ 1 & y_{4j} & y_{4j}^2 & y_{4j}^3 & y_{4j}^4 & y_{4j}^5 \\ 1 & y_{5j} & y_{5j}^2 & y_{5j}^3 & y_{5j}^4 & y_{5j}^5 \end{bmatrix} \begin{bmatrix} H_{0j} \\ H_{1j} \\ H_{2j} \\ H_{3j} \\ H_{4j} \\ H_{5j} \end{bmatrix} = \begin{bmatrix} x_{0j} \\ x_{1j} \\ x_{2j} \\ x_{3j} \\ x_{4j} \\ x_{5j} \end{bmatrix} \tag{6}$$

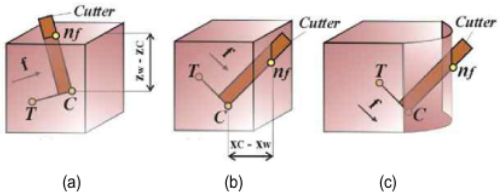

(a) (b) (c)

Fig. 3. Location of UEP: (a) Top surface; (b) straight wall surface; (c) non-straight wall surface.

where (x_{0j}, y_{0j}) ,..., (x_{5j}, y_{5j}) are the coordinates of the given points in a workpiece section. From this equation, the wall surface could be determined whether it is a straight or nonstraight staircase profile.

4. Obtaining engagement points

In this study, the geometry of the cut was calculated by determining two engagement points, LEP and UEP. Initially, LEP was assumed to be located at the bottom of the cutting edge; hence, Eq. (4) could be used with the height of engagement point (l_n) set to zero. For certain conditions, however, LEP's location was not at the bottom side. The details of these conditions are discussed in Sec. 4.3.

The coordinate of UEP was calculated by using Eq. (4) after determining l_n, which was measured from the bottom of the cutting edge to the engagement point. Given the complexity of the tool orientation, the UEP could be found in three possible surfaces: top (Fig. 3(a)), straight wall (Fig. 3(b)), or nonstraight wall surface (Fig. 3(c)). The calculation method for l_n was divided into two. The first was the curve boundary method, which is used when the wall surface is identified as a nonstraight staircase. The second was the cylindrical boundary method, which is used when the engagement point is located on the top surface and on the wall of the straight staircase.

4.1 Cylindrical boundary method

The cylindrical boundary method is a part of ABM [23]. In this study, the method to obtain l_n using the cylindrical boundary method is briefly discussed. The algorithm of this method is more efficient and simpler than that of the curve boundary method. Hence, the former is preferred over the latter when the wall surface is identified as a straight staircase. The cutting tool moves in the x-axis direction; thus, this method was divided into X- and Z-cylindrical methods.

On the one hand, Z-cylindrical method was used when the engagement point was identified on the top surface. Then, l_n was determined on the basis of the z-axis of the workpiece section where the cutter contact point $C(x_C, y_C, z_C)$ is located (Fig. 3(a)).

$$l_n = (z_w - z_C) / \cos\vartheta \tag{7}$$

On the other hand, X-cylindrical method was used when the engagement point was identified on the flat wall surface. The height of the engagement point was determined on the basis of the x-axis of the wall surface next to point $C(x_C, y_C, z_C)$ (Fig. 3(b)).

$$l_n = (x_w - x_C) / \sin\theta_B \tag{8}$$

4.2 Curve boundary method

When the wall surface is identified as a nonstraight staircase, the X-cylindrical method cannot be used to define the UEP. The X-cylindrical method was simpler because the x-axis of the wall surface relative to the y- and z-axes was fixed, which means that the x-axis of the engagement point at any point on the wall surface is similar. The engagement point on the nonstraight surface occurred when x'_{S_C}, y'_{S_C} in Eq. (4) is equal to x_j, y_j in Eq. (5). Then, l_n was defined using the curve boundary method. The coordinate of x'_{S_C}, y'_{S_C} expanded from Eq. (4) is expressed as

$$x'_{S_C} = R\sin\varphi\cos\theta_B + l_n\sin\theta_B + x_T\,, \tag{9}$$

$$y'_{S_C} = R\cos\varphi\sin\theta_A\sin\theta_B + R\cos\varphi\cos\theta_A - l_n\sin\theta_A\cos\theta_B + y_T\,. \tag{10}$$

To simplify the calculation, some parts of x'_{S_C} and y'_{S_C} in Eqs. (9) and (10) were represented as

$$a = R\sin\varphi\cos\theta_B + x_T \tag{11}$$

$$b = R\cos\varphi\sin\theta_A\sin\theta_B + R\cos\varphi\cos\theta_A + y_T\,. \tag{12}$$

Then, x'_{S_C} and y'_{S_C} in Eq. (9) became

$$\begin{bmatrix} x'_{S_C} \\ y'_{S_C} \end{bmatrix} = \begin{bmatrix} a + l_n\sin\theta_B \\ b - l_n\sin\theta_A\cos\theta_B \end{bmatrix}. \tag{13}$$

The value of l_n was determined by inserting the value of x'_{S_C} and y'_{S_C} from Eq. (13) into x_j and y_j in Eq. (5). Then, Eq. (5) could be written as

$$\begin{aligned} a + l_n\sin\theta_B = {} & H_0 + H_1(b - l_n\sin\theta_A\cos\theta_B) + \\ & H_2(b - l_n\sin\theta_A\cos\theta_B)^2 + \\ & H_3(b - l_n\sin\theta_A\cos\theta_B)^3 + \\ & H_4(b - l_n\sin\theta_A\cos\theta_B)^4 + \\ & H_5(b - l_n\sin\theta_A\cos\theta_B)^5\,. \end{aligned} \tag{14}$$

This equation could be rearranged as

$$0 = K_0 + K_1 l_n + K_2 l_n^2 + K_3 l_n^3 + K_4 l_n^4 + K_5 l_n^5\,, \tag{15}$$

where

$$K_0 = H_0 + H_1 b + H_2 b^2 + H_3 b^3 + H_4 b^4 + H_5 b^5 - a \,, \quad (16)$$

$$K_1 = \left(-H_1 - 2H_2 b - 3H_3 b^2 - 4H_4 b^3 - 5H_5 b^4\right)\sin\theta_A \cos\theta_B - \sin\theta_B \,, \quad (17)$$

$$K_2 = \left(H_2 + 3H_3 b + 6H_4 b^2 + 10H_5 b^3\right)\sin\theta_A \cos\theta_B \,, \quad (18)$$

$$K_3 = \left(-H_3 - 4H_4 b - 10H_5 b^2\right)\sin\theta_A \cos\theta_B \,, \quad (19)$$

$$K_4 = \left(H_4 + 5H_5 b\right)\sin\theta_A \cos\theta_B \,, \quad (20)$$

$$K_5 = \left(-H_5\right)\sin\theta_A \cos\theta_B \,. \quad (21)$$

l_n is the root of the fifth-degree polynomial and could be simply defined using a computer application.

$$l_n = roots\left[K_5 \quad K_4 \quad K_3 \quad K_2 \quad K_1 \quad K_0\right] \quad (22)$$

4.3 Cut geometry calculation

The mechanism to define the height of the engagement point starts by identifying two workpiece sections that might engage with the cutting tool at every instantaneous tool position. The workpiece sections were identified by comparing the coordinate of x_C from $C(x_C, y_C, z_C)$ with the coordinate of the curve surface x_j in Eq. (5). x_j was calculated by setting $y_j = y_C$. Sec. A was selected when $x_C > x_j$. Meanwhile, Sec. B was a workpiece section located either after Sec. A (if θ_B positive) or before Sec. A (if θ_B negative).

To reduce the computational time, l_n was initially determined by considering that the engagement point was on the top of Sec. A (S_A). Then, l_n was calculated using the Z-cylindrical method (Eq. (7)). After determining l_n, the initial UEP $n_i\left(x_{n_i}, y_{n_i}, z_{n_i}\right)$ could be calculated using Eq. (4). The correctness of the initial UEP was then checked by defining x_j in Eq. (5) using the assumption that $y_j = y_{n_i}$. If the value of θ_B was positive, then x_j was defined by assuming that the engagement point was on the curve surface of Sec. B (W_B). Then, x_j was changed to x_{jB}. Otherwise, the engagement point was assumed to be on the curve surface of Sec. A. In this case, x_j was defined using the curve equation of Sec. A, which is denoted by x_{jA}.

The initial UEP is incorrect if $x_{n_i} < x_{jA}$ when θ_B negative or $x_{n_i} < x_{jA}$ when θ_B was positive. Hence, the final UEP $n_f\left(x_{n_f}, y_{n_f}, z_{n_f}\right)$ should be recalculated. n_f could be located either on the curve wall of Sec. A (W_A), on the curve wall of Sec. B (W_B), or on the top of Sec. B (S_B). To define the final location, the engagement points when the contact is on the wall surface (i.e., $n_w\left(x_{n_w}, y_{n_w}, z_{n_w}\right)$) should be defined using the height of engagement point on the wall surface (l_w). Lastly, the procedures to obtain the engagement points when the presumption is incorrect should be implemented. All cases are illustrated in Figs. 4 and 5, and the methods to determine the final height of the engagement point are summarized in Table 1. l_A and l_B are the heights of the engagement point when located at S_A and S_B, respectively.

The method for calculating the cut geometry was developed to support the data for the calculation of the cutting force. Machining optimization was performed on the basis of the cut area data generated at any instantaneous tool location. Cut area data comprised the length and thickness of the cut. After obtaining the length of cut, the cut thickness should be determined. Kiswanto et al. [23] mentioned that the cut thickness of the perpendicular tool orientation was defined as the distance between the current and previous tooth paths. However, machining a complex part surface in five-axis milling normally considers the tool inclination angle (α). When the tool has an inclination angle, the cut thickness becomes smaller than the distance of the two consecutive tooth paths. Therefore, the

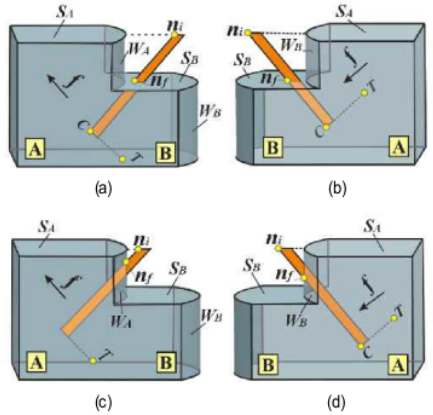

Fig. 4. Location of UEP when $z_A > z_B$.

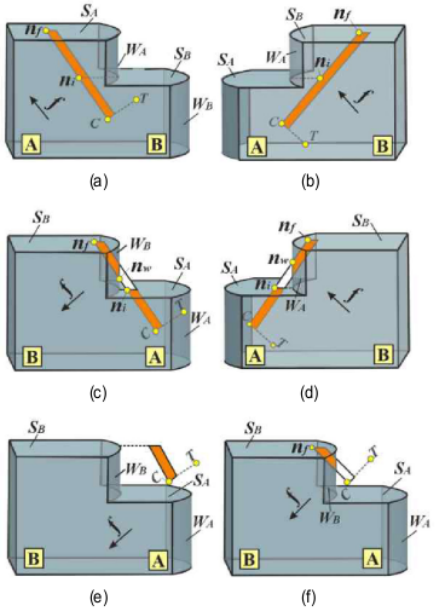

Fig. 5. Location of UEP when $z_A < z_B$.

Table 1. Process to identify engagement location and calculate l_n.

No.	Indication	Location engagement point	l_n
$z_A > z_B$			
A.1	$x_{n_i} < x_{jA}$, $z_{n_i} > z_B$, $z_{n_w} < z_B$	S_B (Fig. 4(a))	$l_n = l_B$
A.2	$x_{n_i} > x_{jB}$, $z_{n_i} > z_B$, $z_{n_w} < z_B$	S_B (Fig. 4(b))	$l_n = l_B$
A.3	$x_{n_i} < x_{jA}$, $z_{n_i} > z_B$, $z_{n_w} > z_B$	W_A (Fig. 4(c))	$l_n = l_w$
A.4	$x_{n_i} > x_{jB}$, $z_{n_i} > z_B$, $z_{n_w} > z_B$	W_B (Fig. 4(d))	$l_n = l_w$
$z_A < z_B$			
B.1	$x_{n_i} > x_{jB}$, $z_{n_w} < z_A < z_B$ and $z_C < z_A$	S_B (Fig. 5(a))	$l_n = l_B$
B.2	$x_{n_i} < x_{jA}$, $z_{n_w} < z_A < z_B$ and $z_C < z_A$	S_B (Fig. 5(b))	$l_n = l_B$
B.3	$x_{n_i} < x_{jB}$, $z_A < z_{n_w} < z_B$ and $z_C < z_A$	W_B and S_B (Fig. 5(c))	$l_n = l_B - (l_w - l_A)$
B.4	$x_{n_i} > x_{jB}$, $z_{n_w} < z_A < z_B$ and $z_C < z_A$	W_A and S_B (Fig. 5(d))	$l_n = l_B - (l_w - l_A)$
B.5	$z_C > z_A$ and $z_w > z_B$	None (Fig. 5(e))	$l_n = 0$
B.6	$z_C > z_A$ and $z_w < z_B$	S_B (Fig. 5(f))	$l_n = (l_B - l_A)$

inclination angles should be considered in the cut thickness calculation. The cut thickness (h) as a function of tool rotation angle is defined as

$$h = f \sin\varphi \cos\alpha , \tag{23}$$

where f is the feed rate.

Lastly, the cut area (A) was determined by multiplying the length and thickness of the cut.

$$A = l_n . h \tag{24}$$

5. Implementation and discussion

A MATLAB simulation program based on the derived formulae was developed. For validation purposes, the tests were performed using two complex surfaces (Figs. 6(a) and (b)). The workpiece material was produced through 2.5D rough milling. The machining for the first test was performed using a two-teeth flat-end cutter with a diameter of 12 mm and an inclination angle of 10°. The machining conditions for model test 1 are as follows: feed rate = 0.1 mm/tooth and spindle speed = 4000 rpm. For test 2, the same cutter was utilized, but the diameter was 14 mm and the inclination angle was 5°. The feed rate and spindle speed were 0.15 mm/tooth and 4000 rpm, respectively. The tests were performed for a full-immersion milling cutter process (tool rotation angle = 180°). The ability of the simulation program to provide the cut geometry data, including the method to verify the accuracy, is discussed in the subsequent subsection. Moreover, the performance of the proposed method in solving the issue on the long computational time is compared with that of the Z-mapping method.

5.1 Cut geometry calculation

The geometry and length of the cut could be generated through the simulation program. The geometry for model tests 1 and 2 are presented in Figs. 6(c) and (d), respectively. These figures display the shape of the cut corresponding to the shape of the remaining material that should be removed to obtain the expected part surface. The results indicated that the proposed method was accurate. The length of cut for one tool pass generated by the simulation program are displayed in Figs. 6(e) and (f). The complexity of the workpiece surface and tool orientation changed because the part surface caused fluctuations in the length of cut.

The simulation program could also generate the cut geometry data for one tool rotation. Four samples of the length of cut from the two cutter contact points in every model test are presented in Figs. 7(a)-(d), and the cut area data are shown in Figs. 7(e)-(h). All tests demonstrated that the length of cuts and the cut area fluctuated. The graphs of the cut area were significantly different from the graph of the length of cut, indicating that the cut thickness exerted a significant effect to the cut area.

The developed simulation program could also be used to determine the depth of the cut, which is defined as the distance between the lowermost part of LEP and the uppermost part of UEP in one tool rotation relative to the z-axis of the GCF. The depths of the cut for model tests 1 and 2 were within 1.78-7.32 and 2.68-6.38 mm.

To examine the accuracy of the proposed method, the geometry of cuts for one tool rotation obtained using the simula-

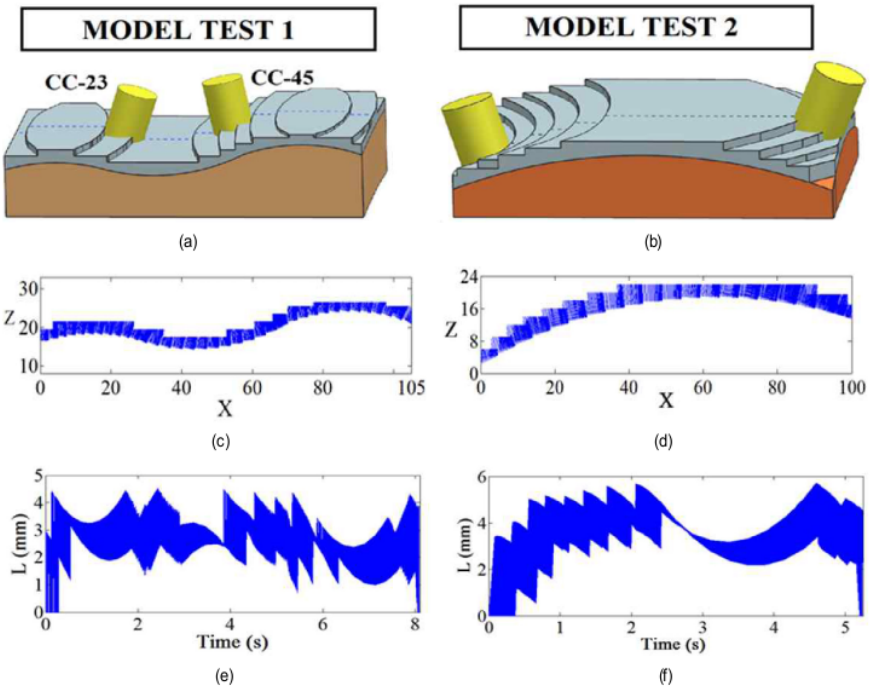

Fig. 6. (a) Model test 1; (b) model test 2; (c) shape of cut (model test 1); (d) geometry of the cut (model test2), and progression of the length of cut for model tests (e) 1; (f) 2.

tion program (Figs. 7(i)-(l)) were compared with those obtained using Siemens-NX (Figs. 7(m)-(p)). The result of the latter was obtained by extracting the intersection model of the cutting tool and the workpiece. The result clearly demonstrated that the geometry of the cut obtained using the program simulation corresponded to the one generated using Siemens-NX. The findings indicated the accuracy of the proposed method.

5.2 Model verification

Although the test results showed that the proposed method is applicable and accurate, a validation test should still be performed. The method was verified by comparing the length of cut calculated using the proposed algorithm with that obtained using Siemen-NX. The coordinates of the engagement points were checked using the intersection model of the cutter and the workpiece (Fig. 8(a)). The intersection model was extracted by placing and orienting the cutting tool at the targeted position based on the cutter location data. Then, the intersection model was extracted. To measure the length of cut, the front sides of the cutting tool model was modified (Fig. 8(a)). Provided that the intersection model was extracted, the coordinate of engagement points could be obtained, and the height of engagement point could be measured. The length of cut for CC-22 of model test 2 and that for CC-23 of model test 1 were verified.

To obtain a detailed analysis on the model verification, the CWEs were separated into several segments with respect to the location of the upper engagement point. The engagement location was divided into seven segments (Fig. 8(b)). Segments A, C, E, and G were the segments when UEP was located on the top of the workpiece section. Meanwhile, the engagement points in segments B and F were the engagement points on the nonstraight wall surface. Segment D depicts the geometry of the cut when UEP was located on the straight surface. The deviation for every segment is presented in Fig. 8(c). The error was calculated by dividing the deviation between the length of cut obtained from the simulation program and that from Siemen-NX $\left\{error = \left(l_{(ABM)} - l\right) / l_{(NX)}\right\}$. CC-23 was divided into five segments (Fig. 8(d)). As previously stated, segments A, C, and E are the segments when the engagement point is on the top surface, whereas segments B and D are those when the engagement point is on the wall surface. The verification result for CC-23 is displayed in Fig. 8(e).

The proposed method could be used to determine the length of cut with high accuracy when the cutting tool engaged with the workpiece is on the top of the section and the flat wall surface. The test showed that the error was minimal or negligible. Relatively higher errors (less than 6 %), however, appeared

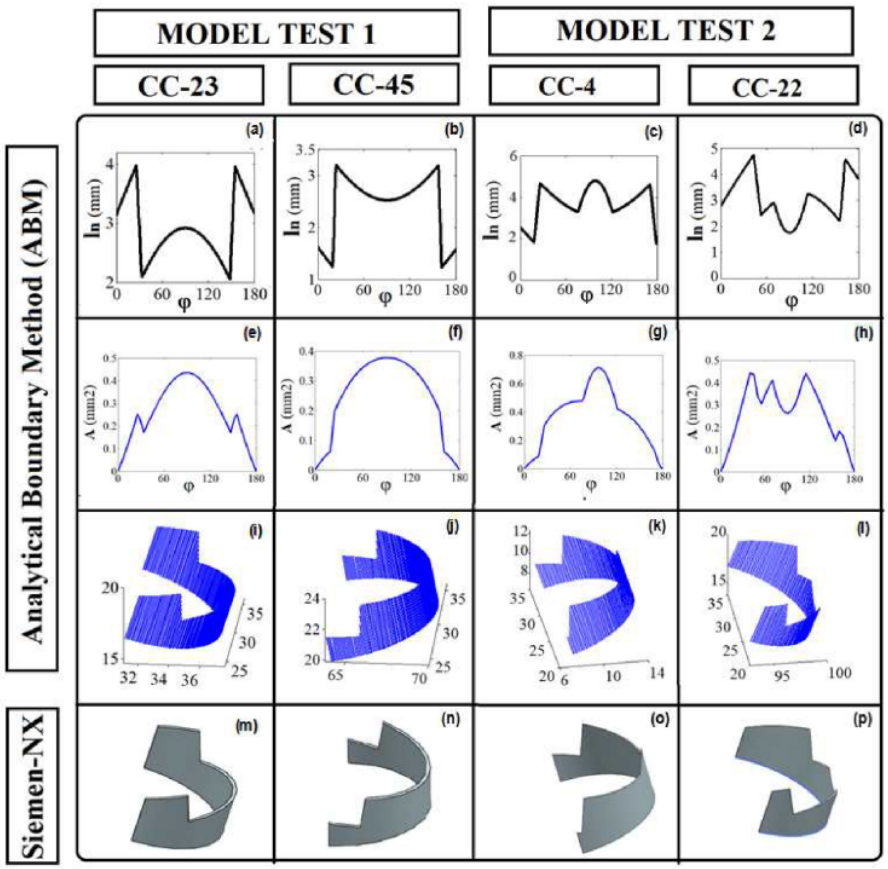

Fig. 7. Shape and size of the cut for one tool rotation.

when the engagement points were located on the nonstraight surface. The deviation obtained due to the curved-wall surface was approximately defined using the polynomial method. For the approximation approach, the accuracy largely depended on the accuracy definition of the curve profile. A series of tests confirmed the accuracy of the proposed algorithm.

5.3 Computational time comparison

The major advantage of the analytical approach in comparison with other methods, such as the solid model and discrete method, is its efficient computation [21, 23]. Therefore, to ensure the efficiency of the proposed method, the computational time of the method was compared with that of the Z-mapping method. Z-mapping is a discrete method in which the discrete number of the grid size largely influences the accuracy. High resolutions result in not only high accuracy but also long computation time and vice versa. By contrast, the analytical method has no correlation with grid size and computational time.

For comparison purposes, the engagement data for the part model and the workpiece surface shown in Fig. 6(a) was calculated using the Z-mapping method. The test was performed using similar machining conditions and cutting tool geometry. In this test, the grid size of the workpiece surface was set to 0.2 mm. The computational time was tested using MATLAB on an Intel Core i7 2.7 GHz computer with 16 GB RAM. The test was performed uninterrupted during the cutting, followed by 53 cutter contact points in one tool pass. The results, were the average value after three time measurements for each method (Fig. 9).

The graph in Fig. 9 clearly displays that the computational time of the Z-mapping method was higher than that of the proposed method. The proposed method consumed only 713.87 *s* to calculate the geometry of the cut (Fig. 6(e)), whereas Z-mapping consumed 2633.65 *s*. This large difference because the Z-mapping method checked and updated large data.

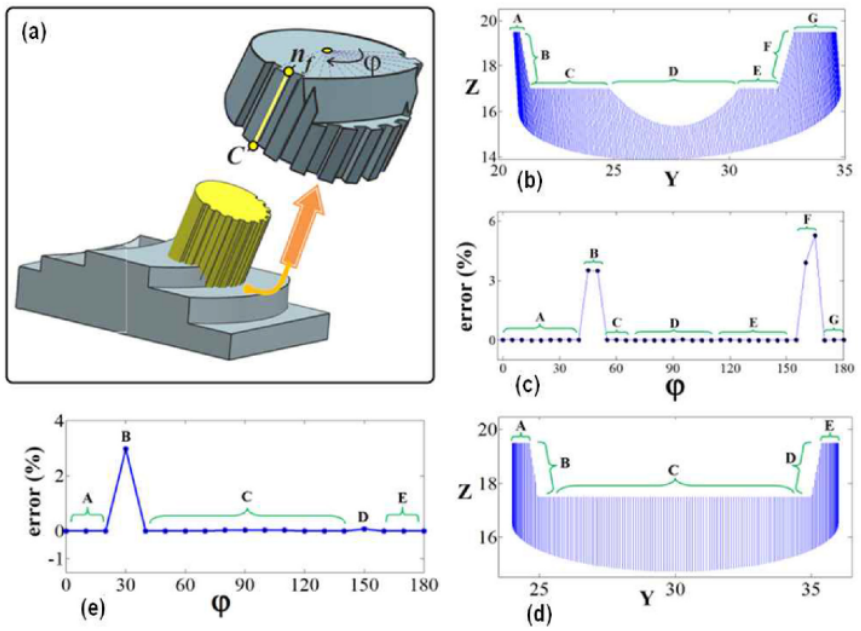

Fig. 8. Model verification: (a) Results of the siemen-NX; (b) shape of cut CC-22 (model test 2); (c) error of CC-22; (d) shape of cut CC-23 (model test 1); (e) error of CC-23.

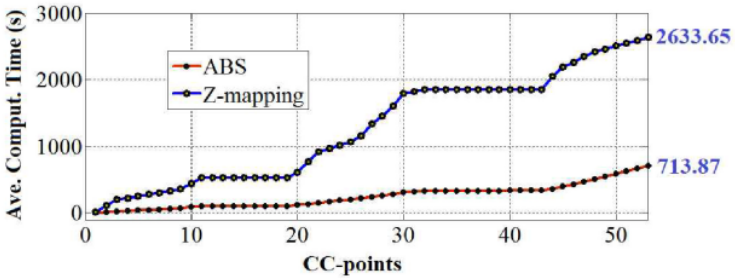

Fig. 9. Computational time of the proposed and Z-mapping methods.

6. Conclusions

An extended ABM for defining instantaneous cut geometry during semifinish milling was developed in this study. ABM is applicable for straight and nonstraight staircase workpiece surfaces. The engagement point on the nonstraight staircase workpiece was calculated using a method called curve-boundary method. The proposed method was tested using two parts with different surface profiles. Results demonstrated that the proposed method can define the instantaneous cut geometry. The accuracy of ABM was validated by comparing the length of the cut generated using ABM with that generated using Siemen-NX. Moreover, the output of the proposed method was accurate when the tool engaged with the workpiece on the top of the section and on the straight wall section. Relatively small errors were produced when the engagement point was on a nonstraight surface. Moreover, the test proved that the ABM is cheaper than Z-mapping in terms of computational time.

In this study, the effect of the helical angle on the length cut was not considered. The helical angle is crucial in actual machining processes because it changes the CWE. Therefore, the proposed method will include the helical angle in the calculation in future studies.

Acknowledgments

The author would like to thank the Indonesian Ministry of Re-

search Technology and Higher Education for the financial support provided through the fundamental research grant scheme.

Nomenclature

GCF : Global coordinate frame
TCF : Tool coordinate frame
LCF : Local coordinate frame
CWE : Cutter workpiece engagement
UEP : Uppermost engagement point
LEP : Lowermost engagement point
CC : Cutter contact
ABM : Analytical boundary method

References

[1] H. U. Lee and D. W. Cho, Development of a reference cutting force model for rough milling feedrate scheduling using FEM analysis, *International Journal of Machine Tools and Manufacture*, 47 (1) (2007) 158-167.

[2] G. Gao, B. Wu, D. Zhang and M. Luo, Mechanistic identification of cutting force coefficients in bull-nose milling process, *Chinese Journal of Aeronautics*, 26 (3) (2013) 823-830.

[3] S. D. Merdol and Y. Altintas, Virtual cutting and optimization of three-axis milling processes, *International Journal of Machine Tools and Manufacture*, 48 (10) (2008) 1063-1071.

[4] S. Wojciechowski, M. Matuszak, B. Powałka, M. Madajewski, R. W. Maruda and G. M. Królczyk, Prediction of cutting forces during micro end milling considering chip thickness accumulation, *International Journal of Machine Tools and Manufacture*, 147 (2019) 103466.

[5] X. Zhang, J. Zhang, B. Pang and W. Zhao, An accurate prediction method of cutting forces in 5-axis flank milling of sculptured surface, *International Journal of Machine Tools and Manufacture*, 104 (2016) 26-36.

[6] M. Nikawa, M. Okada, H. Mori, Y. Fuji and M. Yamashita, Evaluation of machinability in milling by controlling chip thickness using NC simulation, *Journal of Mechanical Science and Technology*, 32 (10) (2018) 4851-4858.

[7] G. Zheng, C. Xiang, L. Li, R. Xu and Y. Tian, Experimental investigation of cutting force, surface roughness and tool wear in high-speed dry milling of AISI 4340 steel, *Journal of Mechanical Science and Technology*, 33 (1) (2019) 341-349.

[8] D. Yip-Hoi and X. Huang, Cutter/workpiece engagement feature extraction from solid models for end milling, *Journal of Manufacturing Science and Engineering*, 128 (1) (2006) 249-260.

[9] I. Lazoglu, Y. Boz and H. Erdim, Five-axis milling mechanics for complex free form surfaces, *CIRP Annals.*, 60 (1) (2011) 117-120.

[10] Y. Boz, H. Erdim and I. Lazoglu, A comparison of solid model and three-orthogonal dexelfield methods for cutter-workpiece engagement calculations in three-and five-axis virtual milling, *The International Journal of Advanced Manufacturing Technology*, 81 (5-8) (2015) 811-823.

[11] W. S. Yun, J. H. Ko, H. U. Lee, D. W. Cho and K. F. Ehmann, Development of a virtual machining system, part 3: Cutting process simulation in transient cuts, *International Journal of Machine Tools and Manufacture*, 42 (15) (2002) 1617-1626.

[12] L. Zhang, J. Feng, Y. Wang and M. Chen, Feedrate scheduling strategy for free-form surface machining through an integrated geometric and mechanistic model, *The International Journal of Advanced Manufacturing Technology*, 40 (11-12) (2009) 1191-1201.

[13] L. Zhang, Process modeling and toolpath optimization for five-axis ball-end milling based on tool motion analysis, *The International Journal of Advanced Manufacturing Technology*, 57 (9-12) (2011) 905-916.

[14] B. K. Fussell, R. B. Jerard and J. G. Hemmet, Modeling of cutting geometry and forces for 5-axis sculptured surface machining, *Computer-Aided Design*, 35 (4) (2003) 333-346.

[15] E. Aras and D. Yip-Hoi, Geometric modeling of cutter/workpiece engagements in three-axis milling using polyhedral representations, *Journal of Computing and Information Science in Engineering*, 8 (3) (2008) 031007.

[16] Z. Yao and A. Joneja, Computing cutter engagement values in milling tessellated free-form surfaces, *Journal of Computing and Information Science in Engineering*, 10 (4) (2010) 041005.

[17] S. K. Gupta, S. K. Saini, B. W. Spranklin and Z. Yao, Geometric algorithms for computing cutter engagement functions in 2.5 D milling operations, *Computer-Aided Design*, 37 (2005) 1469-1480.

[18] B. Ozturk and I. Lazoglu, Machining of free-form surfaces. Part I: Analytical chip load, *International Journal of Machine Tools and Manufacture*, 46 (7-8) (2006) 728-735.

[19] L. T. Tunc and E. Budak, Extraction of 5-axis milling conditions from CAM data for process simulation, *The International Journal of Advanced Manufacturing Technology*, 43 (5-6) 2009) 538-550.

[20] X. Zhang, J. Zhang, B. Pang and W Zhao, An accurate prediction method of cutting forces in 5-axis flank milling of sculptured surface, *International Journal of Machine Tools and Manufacture*, 104 (2016) 26-36.

[21] G. Kiswanto, H. Hendriko and E. Duc, A hybrid analytical-and discrete-based methodology for determining cutter-workpiece engagement in five-axis milling, *The International Journal of Advanced Manufacturing Technology*, 80 (9-12) (2015) 2083-2096.

[22] O. Hendriko, E. Duc and G. Kiswanto, Analytical method for obtaining cutter workpiece engagement in five-axis milling. Part 3: Flat-end cutter and free-form workpiece surface, *Advances in Sustainable and Competitive Manufacturing Systems* (2013) 705-716.

[23] G. Kiswanto, H. Hendriko and E. Duc, An analytical method for obtaining cutter workpiece engagement during a semi-finish in five-axis milling, *Computer-Aided Design*, 55 (2014) 81-93.

[24] E. Duc and G. Kiswanto, Analytical cut geometry prediction for free form surface during semi-finish milling, *ASME 2013 International Manufacturing Science and Engineering Conference collocated with the 41st North American Manufacturing Research Conference*, American Society of Mechanical Engi-

neers Digital Collection, June 10 (2013).
[25] G. Kiswanto, H. Hendriko and E. Duc, Analytical method for obtaining cut geometry of helical toroidal cutter during semi-finish in 5-axis milling, *Applied Mechanics and Materials,* 541 (2014) 780-784.
[26] H. Hendriko, G. Kiswanto, J. Istiyanto and E. Duc, Implementation of analytical boundary simulation method for cutting force prediction model in five-axis milling, *Machining Science and Technology*, 22 (1) (2018) 163-179.
[27] H. Hendriko, Mathematical model for calculating scallop height of toroidal cutter in five-axis milling, *ARPN Journal of Engineering and Applied Sciences*, 12 (2017) 5642-5646.

Hendriko Hendriko received his doctor's degree in manufacturing technology from Universitas Indonesia, Indonesia, and Universite Clermont, France, in 2014. His main research interest is advanced machining simulation, especially the development of methods to calculate the cut geometry and cutting forces for the optimization of machining parameters in five-axis milling. He is also involved in several research projects involving the development of the kinematics analysis of multiaxis parallel robots.

JMST

ORIGINALITY REPORT

10%	10%	9%	0%
SIMILARITY INDEX	INTERNET SOURCES	PUBLICATIONS	STUDENT PAPERS

PRIMARY SOURCES

1	tel.archives-ouvertes.fr Internet Source	6%
2	Gandjar Kiswanto, Hendriko Hendriko, Emmanuel Duc. "An analytical method for obtaining cutter workpiece engagement during a semi-finish in five-axis milling", Computer-Aided Design, 2014 Publication	4%

Exclude quotes	On	Exclude matches	< 3%
Exclude bibliography	On		